Performance Evaluation of Large Aperture "Polished Panel" Optical Receivers Based on Experimental Data

Victor Vilnrotter
Jet Propulsion Laboratory
4800 Oak Grove Dr.
Pasadena, CA 91109
818-354-4605
Victor.A.Vilnrotter@jpl.nasa.gov

***Abstract*—Recent interest in hybrid RF/Optical communications has led to the development and installation of a "polished-panel" optical receiver evaluation assembly on the 34-meter research antenna at Deep-Space Station 13 (DSS-13) at NASA's Goldstone Communications Complex[1]. The test setup consists of a custom aluminum panel polished to optical smoothness, and a large-sensor CCD camera designed to image the point-spread function (PSF) generated by the polished aluminum panel. Extensive data has been obtained via real-time tracking and imaging of planets and stars at DSS-13. Both "on-source" and "off-source" data were recorded at various elevations, enabling the development of realistic simulations and analytic models to help determine the performance of future deep-space communications systems operating with on-off keying (OOK) or pulse-position-modulated (PPM) signaling formats with photon-counting detection, and compared with the ultimate quantum bound on detection performance for these modulations. Experimentally determined PSFs were scaled to provide realistic signal-distributions across a photon-counting detector array when a pulse is received, and uncoded as well as block-coded performance analyzed and evaluated for a well-known class of block codes.**

TABLE OF CONTENTS

1. INTRODUCTION

The option to provide an optical communications capability for the 34-meter microwave antennas of the Deep-Space Network (DSN) is currently under consideration [1,2]. This concept is predicated on the assumption that existing RF capabilities would not be compromised, hence the new optical reception capability should be added without significantly impacting the RF reflecting surfaces, the backup structure, or the pointing requirements on operational DSN antennas. One way to achieve optical communications requirements is to polish the aluminum panels of the antenna's main reflector to optical smoothness, and employ a suitably large detector array to collect the focused light. This approach would result in a very large collecting aperture if, for example, the inner 26 meters of solid aluminum panels were all polished to optical smoothness. However, the extent to which thin aluminum panels can be shaped and polished to optical requirements remains to be quantified. This paper examines the potential communications performance of a polished panel optical receiver, using experimental data obtained at the Goldstone Communications Complex, with NASA's 34 meter research antenna at DSS-13.

As described in [1, 2], a custom mounting bracket was constructed, and the polished panel mounted on the main reflector of the 34 meter antenna at DSS-13. The spot size, or "point spread function" (PSF) generated by the polished panel at its focal distance was recorded using a 10 mega-pixel Finger Lakes Instruments (FLI) digital camera, mounted next to the subreflector on the movable part of the structure in a weather-proof enclosure, and controlled from a small room located on the DSS-13 antenna called the "alidade". Here we develop, analyze and evaluate the communications performance of a high data-rate optical "polished panel" communications receiver, based on the PSF obtained by tracking bright planets and stars with the 34 meter antenna. The quantum limit for on-off-keying (OOK) and binary pulse-position-modulated (PPM) signals will be determined in the absence of background, characteristic of night-time reception, along with high-background performance when operating during the day. The analytic results are verified via simulation, and performance improvement via block codes on the performance of OOK and binary PPM symbols is evaluated.

[1] Author is with the Jet Propulsion Laboratory, California Institute of Technology. Government sponsorship acknowledged.

978-1-4673-1813-6/13/$31.00 ©2013 IEEE

2. MATHEMATICAL MODEL OF FOCAL-PLANE ARRAY PROCESSING

To facilitate analysis and derive the structure of the estimator, the sensor in the focal plane is modeled as an array of bins as in Fig. 1, and Poisson distribution assumed for the number of photo-electrons generated in each bin in response to the signal intensity. The key features of the focal-plane model are shown in Fig. 1, where an elliptical intensity distribution, or "point-spread function" (PSF), is assumed in response to an optical point-source effectively at infinity such as Jupiter or a bright star. The elliptical shape was selected after it was determined that the Vertex panel generated an elliptical spot, instead of a perfectly circular intensity distribution.

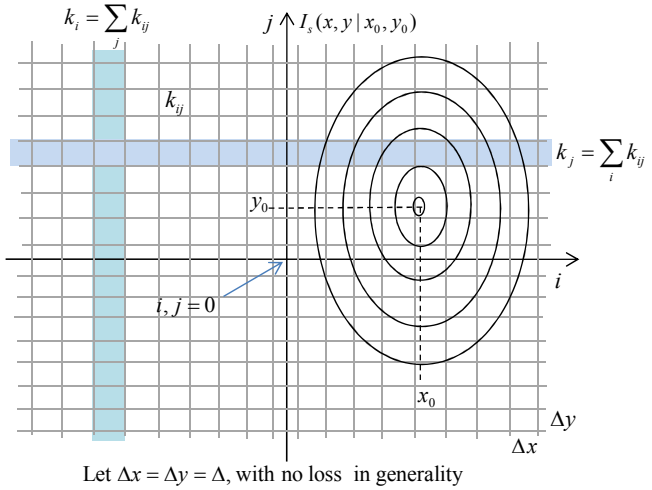

Figure 1. Focal-plane model of pixel array, and elliptical PSF with pointing offsets (x_0, y_0), motivated by experimentally determined point-spread function (PSF) for the high-quality Vertex panel.

For purposes of analysis, the PSF is assumed to be a two-dimensional elliptical Gaussian distribution as shown in Fig. 1, with center at (x_0, y_0):

$$I_s(x, y \mid x_0, y_0) = I_s\,(2\pi\sigma_s^2)^{-1} \times \exp\{-[(x-x_0)^2/2\sigma_x^2 + (y-y_0)^2/2\sigma_y^2]\} \quad (1)$$

in watts/cm^2. The detector elements are taken to be small squares in this model, with power P_{ij} over the *ij* th detector-element equal to the integral of the intensity distribution over its active area. Integrating power over time yields energy, or average "count-intensity" λ_s if the received laser energy is measured in terms of photons or photo-electrons:

$$\lambda_s(i, j \mid x_0, y_0) = \int_0^T P_s(i, j \mid x_0, y_0)\, dt \;\cong T\Delta^2 I_s(i\Delta, j\Delta \mid x_0, y_0) \quad (2)$$

With this model, the photon count from the *ij*-th detector element over a time interval of *T* seconds can be modeled as a Poisson distributed random variable with count probability

$$p(k_{ij} \mid x_0, y_0) = [\lambda_s(i, j \mid x_0, y_0)]^{k_{ij}} \exp[-\lambda_s(i, j \mid x_0, y_0)]/k_{ij}!$$

where k_{ij} is the observed photo-count from the *ij*-th detector element. Recognizing that counts from different detector elements are independent, and defining the vector of counts from the entire array as $\mathbf{k} = \lfloor k_{ij} \rfloor$, the joint probability density of the array of counts becomes:

$$p(\mathbf{k} \mid x_0, y_0) = \prod_{i,j} [\lambda_s(i, j)]^{k_{ij}} \exp[-\lambda_s(i, j)]/k_{ij}! \quad (4)$$

Equation (4) can be used to derive the performance of polished panel optical receivers observing OOK or binary PPM symbols. This is inherently a multi-mode model, however we shall see that with photon-counting detection only the total energy, or total photon count, matters in determining receiver performance.

3. OPTICAL COMMUNICATIONS PERFORMANCE

The Coherent-State Representation of Optical Signals

In order to determine the fundamental quantum limits on detection performance for OOK and PPM signals, it is necessary to introduce notation that is generally used to describe the properties of received laser signals in the limit of small signal energies. Coherent states, representing electromagnetic radiation produced by physical devices such as lasers, are an important class of states for optical communications. It has been shown [3, 4] that coherent states of a single mode of radiation $|\alpha\rangle$ can be represented in the form of a superposition of orthonormal eigenstates $|n\rangle$, known as the number eigenstates:

$$|\alpha\rangle = e^{-\frac{1}{2}|\alpha|^2} \sum_{n=0}^{\infty} \frac{\alpha^n}{(n!)^{1/2}} |n\rangle \quad (5)$$

Each number eigenstate $|n\rangle$ contains exactly *n* photons, and hence the probability of obtaining exactly *n* photons as the outcome of an experiment can be computed as

$$|\langle \rho \mid n\rangle|^2 = \langle n \mid \rho \mid n\rangle = e^{-|\alpha|^2} \frac{|\alpha|^{2n}}{n!} \quad (6)$$

These are recognized as Poisson probabilities for the number of photons, with the average number of photons equal to $|\alpha|^2$. Note that this model is consistent with the detector array model described in Section II, where the output of each detector element in response to a received signal field is Poisson distributed, as in equation (4).

Coherent states are not orthogonal, as can be seen by considering the overlap between two arbitrary coherent states, $|\alpha\rangle$ and $|\beta\rangle$. Orthogonality requires the overlap to vanish, however for coherent states the squared magnitude of the overlap is not zero:

$$|\langle\alpha|\beta\rangle|^2 = \left| e^{-(|\alpha|^2+|\beta|^2)/2} \sum_n \sum_m \frac{\alpha^n}{\sqrt{n!}} \frac{(\beta^*)^m}{\sqrt{m!}} \langle n|m\rangle \right|^2 = \left| e^{-(|\alpha|^2+|\beta|^2-2\alpha\beta^*)/2} \right|^2 = e^{-|\alpha-\beta|^2} \quad (7)$$

Here we made use of the orthogonality of the number states to simplify the intermediate expression. Equation (7) demonstrates that there is always some overlap between coherent states, regardless of how great the average photon count in each state may be.

As shown in [3, 4], the quantum limit on error probability attainable by any pair of binary signals can be expressed in terms of their overlap as:

$$P^*(E) = 1 - P^*(C) = \tfrac{1}{2}\left[1 - \sqrt{1 - |\langle\psi_0|\psi_1\rangle|^2}\right] \quad (9)$$

This expression for the quantum limit is valid for OOK, binary PPM, and all other binary signal-sets. We next consider the two signal types of interest for high data-rate deep-space optical communications, namely OOK and binary PPM.

Quantum limit for OOK and binary PPM signals

For OOK signals, a given T-second symbol-interval either contains a pulse, or contains nothing. The pulse energy is therefore twice the average signal energy, which is the key parameter for deep-space communications. Substituting $|0\rangle$ and $|\alpha\rangle$ for the quantum states under the "off" and "on" hypotheses, respectively. The error probability of the optimum quantum receiver for OOK can be expressed in terms of the average number of photons in the signal averaged over both hypotheses, $K_s = \frac{1}{2}|\alpha|^2$, as

$$P^*_{OOK}(E) = \tfrac{1}{2}\left[1 - \sqrt{1 - |\langle\psi_0|\psi_1\rangle|^2}\right] = \tfrac{1}{2}\left[1 - \sqrt{1 - e^{-|\alpha|^2}}\right] = \tfrac{1}{2}\left[1 - \sqrt{1 - e^{-2K_s}}\right] \quad (10)$$

This result applies only to single-mode pure-state signals, without any background noise fields. The signal-plus-noise problem is quite complicated and will not be treated here.

It is well known that OOK signals are bandwidth-efficient, since one bit of information is transmitted in each symbol-interval. This is not the case for PPM, which suffers from exponential bandwidth expansion. The binary and quaternary PPM symbol-sets are the most bandwidth efficient, requiring only twice the bandwidth of OOK for a given data-rate.

In the quantum formulation, PPM is a product-space signal set, since each slot can be viewed as an independent quantum state. Letting $|\varphi_1\rangle = |\alpha\rangle|0\rangle$ and $|\varphi_2\rangle = |0\rangle|\alpha\rangle$, the square of the overlap for coherent-state binary PPM signals can be evaluated as:

$$|\langle\varphi_1|\varphi_2\rangle|^2 = |\langle 0|\langle\alpha|0\rangle|\alpha\rangle|^2 = |\langle\alpha|0\rangle|^2 |\langle 0|\alpha\rangle|^2 = e^{-|\alpha|^2} e^{-|\alpha|^2} = e^{-2K_s} \quad (11)$$

where now $K_s = |\alpha|^2$ since each slot contains a pulse, hence the average signal energy is equal to the signal energy of either symbol. The quantum limit on binary PPM performance therefore becomes

$$P^*_{2PPM}(E) = \tfrac{1}{2}\left[1 - \sqrt{1 - |\langle\varphi_1|\varphi_2\rangle|^2}\right] = \tfrac{1}{2}\left[1 - \sqrt{1 - e^{-2K_s}}\right] \quad (12)$$

Surprisingly, the ultimate limit on detection performance is the same for OOK and binary PPM signals, under an average power constraint. Since PPM is parameterized with the number of slots, *M*, which is typically taken to be a power of 2, it is important to determine the quantum bound for the general case when higher dimensional PPM signals are used. The quantum limit on the probability of error for PPM signals has been determined earlier in [3], and is given by

$$P^*_{PPM} = \tfrac{M-1}{M^2}\left[\sqrt{1 + (M-1)e^{-K_s}} - \sqrt{1 - e^{-K_s}}\right]^2 \quad (13)$$

As an additional check on equation (12) for binary PPM signals, note that if we let *M* = 2, then equation (13) reduces to equation (12), as follows:

$$P^*_{2PPM} = \tfrac{1}{4}\left[\sqrt{1 + e^{-K_s}} - \sqrt{1 - e^{-K_s}}\right]^2 = \tfrac{1}{4}\left[1 + e^{-K_s} + 1 - e^{-K_s} - 2\sqrt{(1 + e^{-K_s})(1 - e^{-K_s})}\right] = \tfrac{1}{2}\left[1 - \sqrt{1 - e^{-2K_s}}\right] \quad (14)$$

Therefore, when operating under an average power constraint, the ultimate quantum limit on the performance of single-mode OOK and binary PPM signals is identical.

Photon Counting Receiver: OOK signals

Suppose there are two hypotheses, H_0 and H_1, denoting the absence and presence of signal, respectively. If the background radiation can be neglected, then either no

photons or an average of $\lambda = |\alpha|^2 > 0$ photons are received. The received field is assumed to be from a coherent laser, hence the photons are Poisson distributed with conditional densities

$$P(n \mid H_0) = \begin{cases} 1, & n = 0 \\ 0, & n \geq 1 \end{cases}; \qquad P(n \mid H_1) = \frac{\lambda^n}{n!} e^{-\lambda} \tag{15}$$

At the end of each signaling interval the receiver records the total number of detected photons, and decides which hypothesis is true by computing the two likelihood functions $\Lambda_i \equiv P(n \mid H_i), i = 0,1$ and selecting the hypothesis corresponding to the larger of the two. In the absence of noise H_0 is always decoded correctly, therefore $P(C \mid H_0) = P(0 \mid H_0) = 1$. H_1 is decoded correctly if at least one photon is detected: $P(n \geq 1 \mid H_1) = 1 - e^{-\lambda}$. With equal a-priori probabilities, $P(H_0) = P(H_1) = \frac{1}{2}$, the average probability of correct detection becomes

$$P(C) = \sum_{i=1}^{2} P(C \mid H_i) P(H_i) = 1 - \tfrac{1}{2} e^{-\lambda} \tag{16}$$

Finally, the average probability of error is $P(E) = 1 - P(C) = \frac{1}{2} e^{-\lambda}$. With average received signal energy of K_s photons, the average energy of the pulse is $2K_s$, assuming equally likely symbols. The probability of error for OOK in the absence of background, and with average received signal energy K_s, therefore becomes

$$P_{OOK}(E) = \tfrac{1}{2} e^{-2K_s} \tag{17}$$

Note that the exponent is $-2K_s$, which means that the error probability decreases exponentially with $2K_s$.

When background noise is present, the maximum likelihood receiver sets a threshold given by $\eta = 2K_s / \log(1 + 2K_s / K_b)$, and decides H_1 if the signal plus noise counts at the end of the *T* second symbol interval exceeds threshold, otherwise selects H_0 [4]. This threshold increases with K_s, and occasionally takes on an integer value, but this is a set of measure zero and can usually be ignored when calculating the error probability. Ignoring integer threshold values, the probability of correct detection is given by

$$P_{OOK}(C) = \tfrac{1}{2} \left(\sum_{k_0=0}^{\text{floor}(\eta)} \frac{K_b^{k_0} e^{-K_b}}{k_0!} + \sum_{\text{ceil}(\eta)}^{\infty} \frac{(K_b + K_s)^{k_0} e^{-(K_b + K_s)}}{k_0!} \right) \tag{18}$$

hence the error probability in the presence of background is $P_{OOK}(E) = 1 - P_{OOK}(C)$. In summary, the maximum likelihood detection strategy for OOK symbols with Poisson photo-counting is as follows:

The OOK detection strategy can be summarized as follows: sum the photon-counts within the *T*-second symbol-interval, k_0, and compare to the optimal threshold $\eta = 2K_s / \log(1 + 2K_s / K_b)$: if $k_0 < \eta$ declare H_0; if $k_0 > \eta$ declare H_1. Note that k_0 refers to the number of observed counts in an OOK symbol-interval.

Photon Counting Receiver: binary PPM signals

For the case of binary PPM, the maximum likelihood receiver sums photon-counts over both slots, and select the slot with the largest count [4]. In case of count-equalities in the two slots, a random choice is made by tossing a fair coin. In the absence of background a correct decision is made if one or more photons are detected in either slot, an error occurring only if no photons are observed, in which case a random choice is made. With Poisson statistics the probability of observing no photons, given that a pulse with average photon count K_s was actually received, is e^{-K_s}, therefore the average probability of error after a random coin-toss is simply

$$P_{2PPM}(E) = \tfrac{1}{2} e^{-K_s} \tag{19}$$

when the background is negligibly small. The exponent is now $-K_s$, which means that the error probability decreases exponentially with increasing K_s, but it takes twice as much signal energy to achieve the same error probability as with OOK signaling, when photon-counting detection is employed. This is somewhat interesting, in light of the fact that the quantum limit for these two signals sets is identical, given an average signal power constraint.

The above detection strategy for binary PPM does not change with increasing background, although performance degrades. With background, an error is made if the count in the noise-slot exceeds the count in the signal-plus-noise slot: if the counts in the two slots are equal, then a random choice is made by tossing a fair coin. With this strategy, the error probability can be expressed as [4]:

$$P(E) = \sum_{k_1=0}^{\infty} \sum_{k_2=k_1}^{\infty} \gamma(k_1,k_2)\,(K_s + K_b)^{k_1} K_b^{k_2} e^{-(K_s+2K_b)} / k_1!k_2!$$

$$\text{where} \quad \gamma(k_1,k_2) = \begin{cases} 1, & k_1 = k_2 \\ \frac{1}{2}, & k_1 \neq k_2 \end{cases} \qquad (20)$$

To recap, the maximum likelihood strategy for detecting binary PPM symbols with Poisson photo-counting is:

The binary PPM detection strategy can be summarized as follows: sum the photon-counts k_1 and k_2 in the first and second slots, respectively, and compare: if $k_1 > k_2$, declare H_0; if $k_2 > k_1$, declare H_1. In case of a tie, toss a fair coin to determine the outcome.

Note that unlike the integer thresholds discussed for OOK, which is very rare and can be considered a set of measure zero, equalities in slot-counts can now occur with significant probabilities in the presence of noise, hence these count-equalities cannot be ignored. The factor $\gamma(k_1,k_2)$ accounts for the equalities in binary PPM, and have been taken into account when the binary PPM error probabilities were computed.

The above results are illustrated in Fig. 2 for low background, and in Fig. 3 for high background detection. The quantum limit as a function of K_s attains the same error probabilities for both OOK and PPM detection, described by equations (10) and (12), as shown in Fig. 2a, which also shows that in the absence of background ($K_b = 0$) OOK detected via photon counting nearly achieves the quantum limit for all values of K_s. Interestingly, for error probabilities somewhat higher than the average background energy, OOK with photon-counting performs close to the quantum limit as can be seen in Fig. 2a for K_s less than 5, since the probability of detecting a background photon is negligibly small in this region.

For small signal energies the optimum threshold defined above is less than one, hence the detection strategy is equivalent to the noiseless case, namely: declare "no pulse" corresponding to H_0 if no photons are detected, and "pulse detected" corresponding to H_1 if one or more photons are observed.

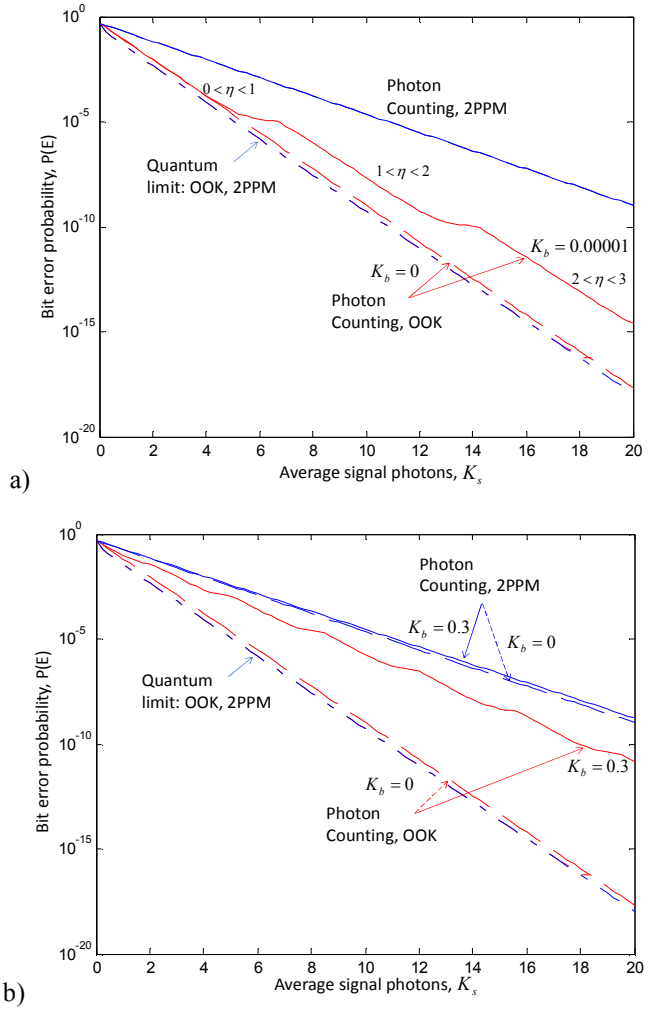

Fig. 2. Quantum limit and photon-counting detection performance of OOK and binary PPM signals as a function of average signal energy K_s: a) extremely low average background energy per symbol-interval, $K_b = 0.00001$; b) low average background energy per symbol-interval, $K_b = 0.3$.

For higher K_s an optimum threshold greater than one must be used, leading to errors if the background generates more photons than the threshold, or if the pulse generates less than threshold: integer changes in the threshold lead to the cusps in the OOK error probability curves seen in Figs. 2a and 2b. With little or no background, OOK detection with photon-counting is "near-optimum" meaning that the error probability exponent is the same as for the quantum limit, and the error probabilities differ only by a factor (of approximately 2) from quantum-limited performance.

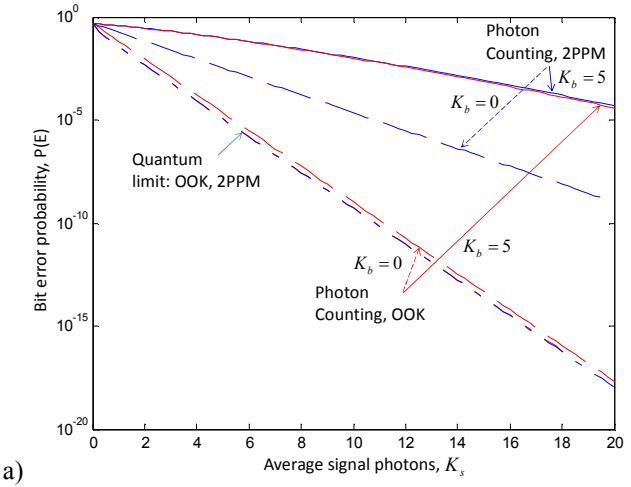

a)

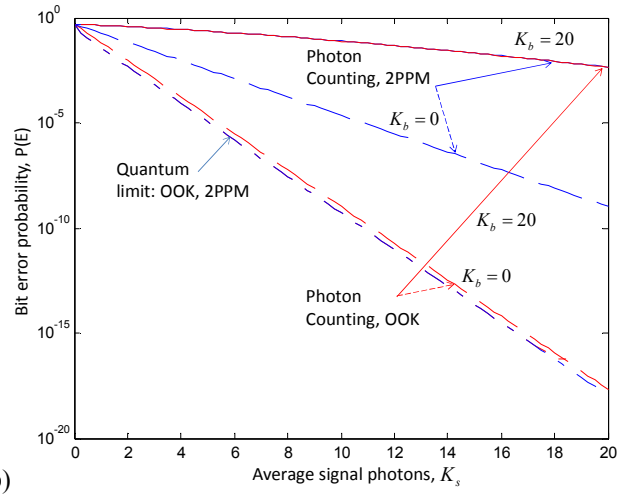

b)

Fig. 3. Quantum limit and photon-counting detection performance of OOK and binary PPM signals as a function of average signal energy K_s: a) moderate average background energy per symbol-interval, $K_b = 5$; b) high average background energy per symbol-interval, $K_b = 20$.

Whereas OOK performs close to the quantum limit in the absence of background, binary PPM with photon-counting performs 3 dB worse, requiring twice the signal energy to achieve a given error probability, since the error probability exponent is a factor of two smaller than for OOK as shown in equation (17). However, there are two slots per binary symbol in a given T-second interval, hence for the same data-rate the background observed in each PPM slot is only half that of OOK. In addition, PPM compares counts in two slots instead of relying on a threshold, as with OOK. These differences in the detection strategy lead to 3 dB worse performance in the noiseless case for PPM , but also lead to less sensitivity to background interference: as can be seen in Fig. 2a, a background rate of 10^{-5} has no observable impact on PPM performance, but degrades OOK performance for high signal energies. Only when the background increases to 0.3 photons per pulse does it begin to degrade PPM performance, as shown in Fig. 2b.

It can be seen in Figs. 3 that for high background counts, the error probability curves for OOK and binary PPM converge, with nearly identical performance for $K_b = 5$ and greater. However, it should be noted that binary PPM requires twice the processing bandwidth of OOK, necessarily leading to wider bandwidth and hence more challenging receiver designs. However, detection of binary PPM relies onn the comparison of counts between adjacent slots and hence does not require the computation of an optimum threshold, which may be troublesome under time-varying background conditions.

Spatial filtering to improve detection performance in the presence of background

As shown in [4], multimode laser fields also lead to Poisson distributed photon-counts, as do single-mode laser fields. With photon-counting direct detection, there is no essential difference between the single-mode and muti-mode models of the photo-counts, both can be described by the Poisson distribution, provided the number of modes is large. In a typical optical communications scenario, the point spread function (PSF) generated by the polished panel consists of a large number of spatial modes, since panel surface imperfections and residual roughness tends to scatter the signal over an area much larger than the diffraction-limited spot-size. Under these conditions, the focal-plane model of the received signal fields can be described by an average field-distribution such as the two-dimensional Gaussian model developed in Section II, and Poisson-distributed counts with average number corresponding to the integrated intensity can be assumed for each detector-element.

With this model of the polished panel receiver, detector array processing can be optimized to achieve best photon-counting performance by sorting the array elements according to energy, and computing the symbol error probability (PSE) for the highest energy detector element, then for the sum of the signal energies in the first two highest energy detectors, and so on, until the minimum PSE is reached. The amount of signal energy collected by the first "*m*" highest-energy detectors will be denoted by

$$K_s(m) = \sum_{n=1}^{m} \lambda_s(n) \qquad (21)$$

where "*n*" is the order index according to signal energy in descending order. In the following performance calculations the background photon distribution is assumed to be uniformly distributed in the detector-plane, hence the amount of collected background energy increases linearly with *m* as more detector elements are included. According to this model, the average number of background photons collected by *m* detector elements is proportional to *m*, $K_b(m) = m\lambda_b$, where λ_b is the average background

photon-count rate per detector element, here assumed to be constant over the array.

As described in [1], the detector array consists of 50X50=2500 elements, but due to camera artifacts the first row and column were deleted, resulting in a 49X49=2401 element square detector array. Error probabilities for OOK and binary PPM have been computed for increasing values of m, using equations (18) and (20), for a given value of average background count rate λ_b and total collected signal energy $K_s(m=2401)$, as defined in equation (21), and with $\lambda_s(n)$ obtained from an experimentally obtained PSF such as the one shown in Fig. 4a, by sorting pixel energies in decreasing order. Writing equations (18) and (20) in terms of $K_b(m)$ and $K_s(m)$ yields

$$P_{OOK}(E) = \tfrac{1}{2}\sum_{\text{ceil}(\eta)}^{\infty}\frac{K_b^k(m)e^{-K_b(m)}}{k!} + \tfrac{1}{2}\sum_{k=0}^{\text{floor}(\eta)}\frac{(K_b(m)+K_s(m))^k\, e^{-(K_b(m)+K_s(m))}}{k!} \qquad (22a)$$

$$P_{2PPM}(E) = \sum_{k_1=0}^{\infty}\sum_{k_2=k_1}^{\infty}\left(\gamma(k_1,k_2)\,(K_s(m)+K_b(m))^{k_1}\times K_b^{k_2}(m)\,e^{-(K_s(m)+2K_b(m))}\right)/k_1!k_2! \qquad (22b)$$

where $\gamma(k_1,k_2)$ has been defined in equation (20). The value of $m=m^*$ that achieves the minimum error probability is determined for binary PPM, as shown in Fig. 4b, for the improved PSF generated by the bright star Vega on Sept. 19th described in [2]. Note that the error probability as a function of m is a smooth curve for binary PPM, but not for OOK due to integer changes in the threshold, as described earlier and shown in Figs. 2. The optimum value of $m=m^*$ can be interpreted as defining a spatial filter that includes only those pixels with energies greater than $\lambda_s(m^*)$, and blocks all others. This approach divides the detector array into two regions, not necessarily contiguous, that blocks signal plus background energy in the "excluded region" from reaching the receiver, as shown in Fig. 4a). This approach will be used to compute bit error probabilities for evaluating coded performance, and will be compared to the simulation discussed in the next section.

4. Binary PPM Simulation Results

The theoretically derived error performance has been verified independently using a simulation program that implemented the binary PPM detection strategy described above, namely:

Binary PPM detection strategy

Sum the photon-counts k_1 and k_2 in the first and second slots, respectively, and compare: if $k_1 > k_2$, declare H_0; if $k_2 > k_1$, declare H_1. In case of a tie, toss a fair coin to determine the outcome.

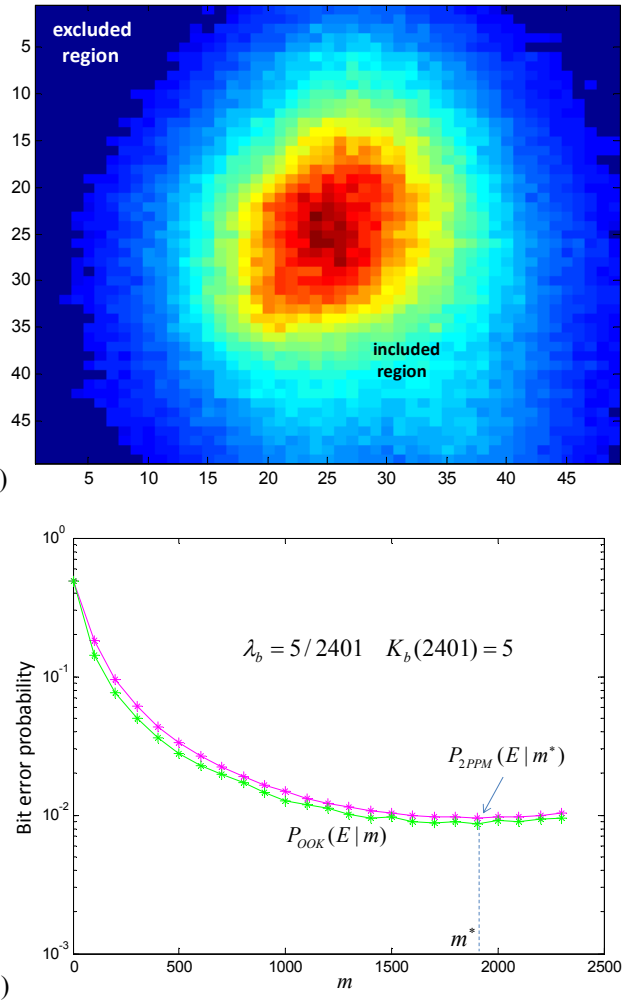

Fig. 4. a) Polished panel PSF generated by the star Vega, showing the low signal energy region excluded by spatial filtering. b) Bit error probability as a function of m for OOK and binary PPM signaling, illustrating the minimum error probability achieved by m^*.

Due to the requirement to generate two large Poisson count-arrays for each symbol, then apply the above algorithm which calls for resolving count-equalities in both slots, it was decided to implement binary PPM detection in this simulation since this was considered to be the more stringent test. The experimentally recorded PSF was used to define the distribution of signal intensity over the detector-

plane, with the total signal energy normalized over the array. To calculate error probabilities as a function of Ks, the total signal energy was multiplied by Ks and the average signal count over each of 49X49=2401 pixels was determined. Next, a Poisson random array was generated, with average count over each pixel given by the experimentally obtained PSF intensity distribution. An illustration of the resulting random count-arrays for various intensities from very high to very low is shown in Fig. 5a) – 5f). Note that for high count-intensities such as in Fig. 5b)-5d), which may correspond to long integration times as would be observed by a narrow-band tracking algorithm such as the one described in [2], the Poisson frame of random array counts resembles the assumed average intensity distribution of Fig. 5a). However, for high-rate data-communications the integration time is necessarily extremely short, hence the random array-counts with an average of 100 signal photons or less no longer resemble the original intensity distribution, as in Fig. 5f).

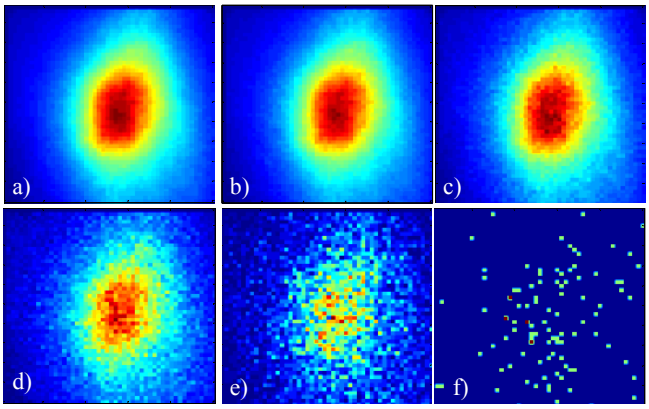

Fig. 5. Illustration of array counts for various pixel-intensity distributions using the experimentally recorded PSF in a) as the average energy distribution, ranging from very high, b), to very low, f), total received signal energy.

The simulation was written for binary PPM, and made use of the experimentally recorded PSF by scaling it to the average number of photons per symbol per array, Ks. An average background intensity of 5 photons per symbol per array was added to the signal distribution, which amounted to 5/2401 background photons per pixel. The background signal intensity was obtained by adding a 1 degree pointing offset in the cross-elevation direction and recording a background frame, so as not to introduce any elevation-dependent errors, an example of which is shown in Fig. 6a) for the case of approximately 100 photons per symbol per slot for illustration purposes.

In the simulation, a Poisson random variable with mean equal to the sum of background and signal intensity was generated for each pixel, the above detection algorithms applied to each of 10,000 realizations of the 49X49 pixel array, and the binary PPM detection strategy was applied for each pair of consecutive frames. Since there is no frame-to-frame memory in the simulation, the signal pulse, hence PSF, was always placed in the first slot. The binary PPM detection strategy was applied, including the randomized selection in case the photo-counts in the two PPM frames were equal, and the number of errors recorded. Each realization of the binary PPM frames was repeated 10,000 times, and the total number of errors divided by 10,000 to obtain an estimate of the bit error rate.

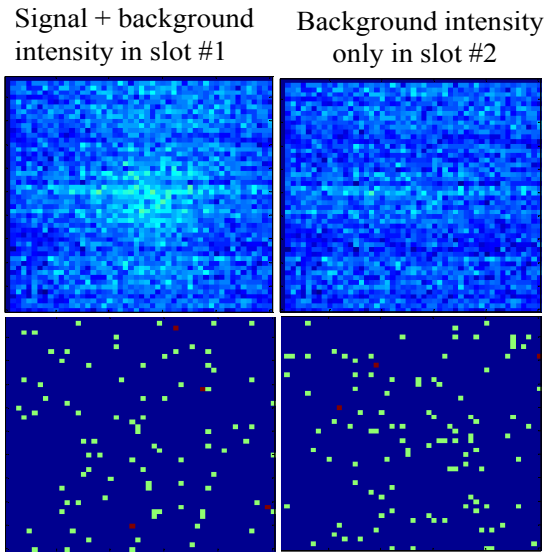

a)

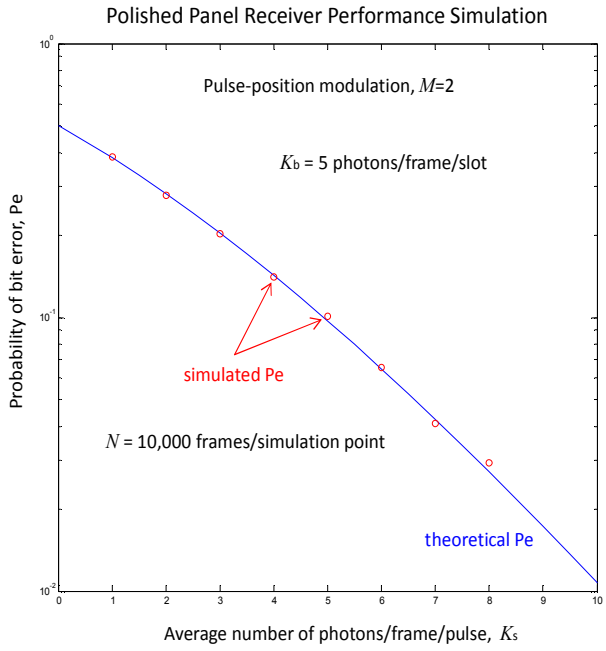

b)

Fig. 6. a) Sample frames of background and signal-plus-background frames, and associated array photo-counts; b) theoretically derived binary PPM performance curve and simulation results.

The results for binary PPM signals are shown in Fig. 6 b), where the entire array was used to detect the signals without any spatial filtering to simplify the simulation, based on the observation that for such low background count-rates nearly the entire array is typically used as shown in Fig. 4a, hence the entire detector array could be considered a spatial filter for this simulation.

The simulation results are shown as red circles in Fig. 6b), whereas the computed error probability is represented by the solid blue line. This simulation required the generation of two $49 \times 49 = 2401$ dimensional Poisson random arrays for each slot, followed by the application of The close agreement between the computed and simulated results provides strong validation of the computed error probabilities for binary PPM signals, supporting the validity of the signal model and detection strategy developed above for computing error probabilities for binary PPM signals.

5. Coding to Improve Detection Performance

The polished panel optical receiver with its inherently large collecting aperture is capable of capturing a large number of signal photons and concentrating it into a small (but not diffraction-limited) spot, performs exceptionally well when the background radiation is negligible, such as during night-time operation. In fact, OOK modulation with simple photon-counting detection closely approaches the quantum-limit on error probability under these conditions, which means that no other detection technique, including much more complex phase-sensitive coherent detection, could perform better than photon-counting OOK. As shown in Fig. 2, uncoded OOK achieves bit error probabilities of $10^{-5} - 10^{-6}$ with average pulse energies of only 6-12 photons, hence very high-rate communication is possible with nominal optical transmitter designs that are capable of delivering 100 signal photons or more as discussed in [2], from 1 astronomical unit or even greater interplanetary distances. However, during daytime operation background increases significantly, especially when pointing close to the sun, leading to background counts of 10-100 photons per slot or more, greatly degrading uncoded detection performance as shown in Fig. 3. Under high background conditions, detection performance for both OOK and binary PPM degrades significantly, to the point where the receiver is unable to achieve the error probabilities required for deep-space optical communications. As shown in Fig. 3, with only 20 background photons per pulse, only bit error probabilities of $10^{-1} - 10^{-2}$ can be reached with either modulation formats, which is not sufficient for deep-space communications where bit error probabilities of 10^{-6} or even lower are routinely required. Some form of coding must be employed in order to improve polished panel receiver performance, under high background operating conditions.

Our goal here is to demonstrate that deep-space communications requirements can be maintained with polished panel type optical receivers even in high background environments through the use of coding, and develop a simple approach to estimate the coded performance of high-rate modulations such as OOK and binary PPM. In Fig. 7, the conditional error probabilities for OOK detection are seen to be nearly equal for $K_b = 20$, and become essentially equal for higher backgrounds, hence a binary symmetric channel (BSC) model is a good approximation even for this asymmetric signal-set. Binary PPM is inherently symmetric, therefore a BSC model is valid for this modulation format when the background energy is sufficiently high.

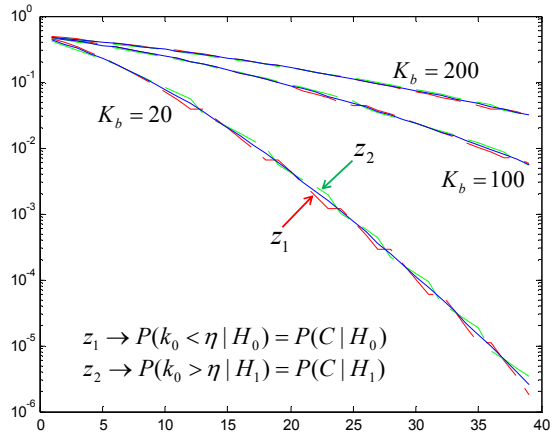

Fig. 7. Conditional error probabilities for equally probable OOK signals with increasing background, demonstrating the validity of binary symmetric channel model.

For the BSC channel, coding can be used to improve receiver performance, when operating in high background environments characteristic of daytime operation. Sequences of k consecutive symbols can be converted into codewords by appending $(n\text{-}k)$ parity-check bits, thus yielding codewords of length n, and forming an (n, k) code. Codewords of length n contain only $k < n$ information symbols: this means that the binary symbol-lengths must be decreased by the code-rate k / n in order to maintain a given data-rate. With an average power constraint, this also implies that the average pulse energy must be decreased by the code-rate k / n in order to maintain an average received signal power. That is, instead of receiving K_s photons per pulse as in the uncoded case, in the block coded system the average pulse energy is smaller by a factor of k / n since the $k K_s$ photons originally distributed among kT seconds must now be distributed among $nT > kT$ seconds: indeed, $n(k/n)K_s = kK_s$, as required. The transition probabilities p are therefore computed with average photon counts of $(k/n)K_s$ at each value of K_s, to account for the additional $(n\text{-}k)$ parity-check bits which must also be

detected, but without causing a decrease in the information throughput of the receiver.

For bounded distance decoders that correct all combinations of t or fewer errors, where t is the greatest integer less than or equal to $(d_{\min}-1)/2$ and $d_{\min}$ is the minimum distance of the code, the exact decoded bit error probability typically depends on the specific code and the decoder, but it can be expressed approximately as

$$P_B(E) = n^{-1} \sum_{j=t+1}^{n} \beta_j \binom{n}{j} p^j (1-p)^{n-j} \tag{23}$$

where β_j is the average number of symbol errors remaining in the corrected sequence given that the channel caused $j > t$ errors, and where p is the transition probability for either OOK or binary PPM, as discussed above. This expression was originally derived by Odenwalder in [5], who argues that for systematic codes $\beta_j \cong j$ is a good approximation. For example, table 4.2 [5] shows that for extended Golay codes $\beta_j \cong j$ in most cases, confirming this approximation. We shall use the expression in (23) with $\beta_j = j$ to approximate the performance gains afforded by systematic block codes, when applied to OOK and binary PPM symbols in the high-background regime:

$$P_B(E) \cong n^{-1} \sum_{j=t+1}^{n} j \binom{n}{j} p^j (1-p)^{n-j} \tag{24}$$

Applying the identity derived in [6] for $t = 1$, namely

$$n^{-1} \sum_{j=2}^{n} j \binom{n}{j} p^j (1-p)^{n-j} = p + p(1-p)^{n-1}$$

equation (24) can be re-written for $t > 1$ as follows:

$$n^{-1} \sum_{j=t+1>2}^{n} j \binom{n}{j} p^j (1-p)^{n-j} =$$

$$n^{-1} \sum_{j=2}^{n} j \binom{n}{j} p^j (1-p)^{n-j} - n^{-1} \sum_{j=2}^{t} j \binom{n}{j} p^j (1-p)^{n-j} =$$

$$p - p(1-p)^{n-1} - (n-1)p^2(1-p)^{n-2} - \frac{(n-1)(n-2)}{2!} p^3 (1-p)^{n-3}$$
$$- \frac{(n-1)(n-2)(n-3)}{3!} p^4 (1-p)^{n-4} \ldots$$
$$- \frac{(n-1)(n-2)\cdots(n-[t-1])}{(t-1)!} p^{t-1} (1-p)^{n-(t-1)}$$

$$= p - p \sum_{j=0}^{t-1} \binom{n-1}{j} p^j (1-p)^{n-1-j} =$$

$$p\left[1 - C_{bin}(t-1, n-1, p)\right] = P_b(\mathrm{E}) \tag{25}$$

where $C_{bin}(t-1, n-1, p)$ is the cumulative distribution function of a binomial random variable with (n-1) degrees of freedom, from zero to t-1, and transition probability p as described above. The last equality in equation (25) is in a form that is particularly easy to compute, since the cumulative distribution of a binomial random variable is readily available in MATLAB and other popular computer applications. Note that the bit error probability in equation (25) can also be expressed as

$$\begin{aligned} P_b(E) &= p\left[1 - C_{bin}(t-1, n-1, p)\right] \\ &= p\left\{ \sum_{j=t}^{\infty} \binom{n-1}{j} p^j (1-p)^{n-1-j} \right\} \end{aligned} \tag{26}$$

which suggests the interpretation that uncoded binary error probability p is decreased by a factor equal to the probability of t or more errors ocurring among n-1 slots.

The performance gains afforded by block codes with hard-decision decoding, has been evaluated by comparing the uncoded performance of OOK and binary PPM for moderately high background counts corresponding to $K_b = 40$, with the performance of well-known BCH codes of various codeword lengths n and various error-correcting capabilities t, and the average signal and background energies scaled according to the code-rate to keep the data-rate and average signal power constant. The results are shown in Figs. 8 as a function of the codeword size n for a fixed value of the error correcting capability t = 2, and in Fig. 9 as a function of t, for a given codeword length n = 63.

Note that for low signal energies below approximately 22 photons the uncoded receiver actually performs slightly better in both cases, but that after exceeding this "threshold" energy the performance of the coded receiver begins to improve dramatically, both as a function of n with constant error-correction t = 2 as in Fig. 8, and with constant codeword length n = 63 for increasing t, as in Fig. 9. The performance of OOK and binary PPM was nearly identical in all cases, hence only the PPM error probabilities were shown in Figs. 8a) and 9a).

In both Figs. 8a) and 9a), the solid blue curve corresponds to the uncoded performance of OOK and binary PPM, and the dashed red curves correspond to coded performance, where equation (25) was used to determine the bit error probabilities. The dashed black curve shows an interesting reversal in the trend as either n or t increases past an "optimum" point, as discussed subsequently. Note that with 40 background photons per symbol, uncoded performance can only achieve $P_b(E) \cong 10^{-4}$ in the range of K_s shown, $0 < K_s < 40$, hence the receiver cannot reach bit error probabilities of 10^{-6} or less, which is usually required for deep-space communications. Table 5.2 in [6] was used to determine n, k and t for BCH codes, in the following discussion.

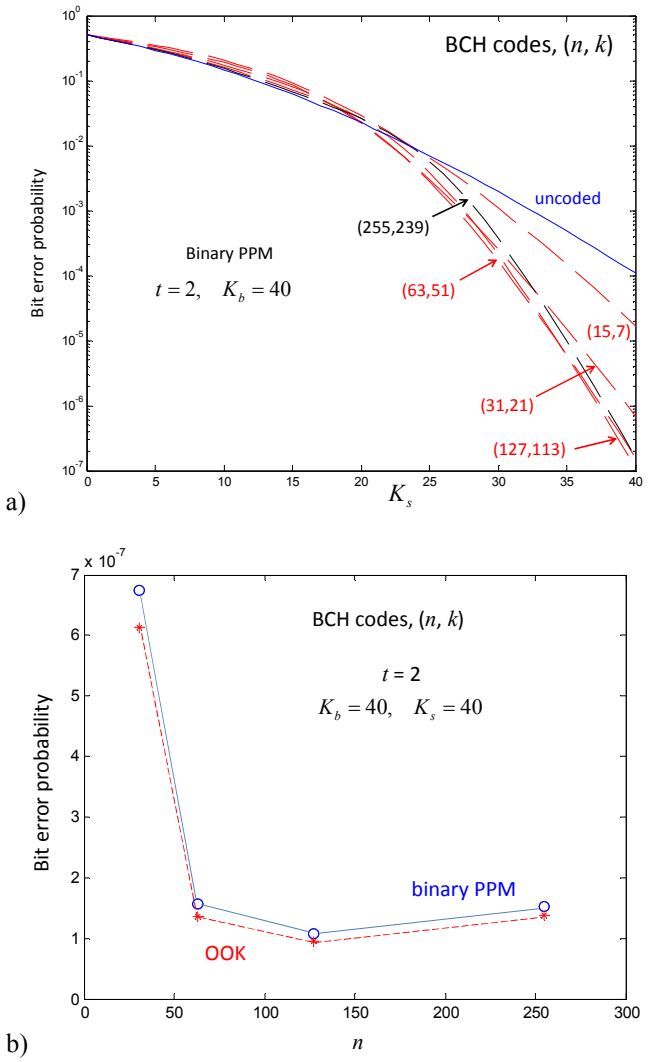

Fig. 8. a) Uncoded and BCH block-coded performance of binary PPM symbols for increasing codeword-length, with $t = 2$; b) minimum error probability achieved with $n = 127, t = 2$.

It can be seen in Fig. 8a) that as the codeword length n increases from 15 to 31 to 63, with the number of information symbols k selected to keep $t = 2$, performance continues to improve but reaches a minimum at $n = 127$ and actually reverses the trend and begins to degrade with $n = 255$ in this region, as the dashed black curve indicates. This reversal begins to occur near the threshold in Fig. 7a, around a bit-error probability of 0.01, and it is attributed to the fact that more than two errors begin to occur in the uncoded sequence within 255 symbols, as the solid blue curve shows around the coding threshold, hence correcting only 2 errors within 255 symbols on the average tends to leave uncorrected errors in these long sequences, degrading performance even as the scaled value of K_s increases with increasing codeword length.

This phenomenon is clearly demonstrated in Fig. 8b, where the bit error performance of both modulations are shown around the optimum point of $n = 127$ at an average signal energy of $K_s = 40$. On this magnified scale the difference between the two modulation schemes can be clearly seen, with OOK performing slightly better than binary PPM in this region.

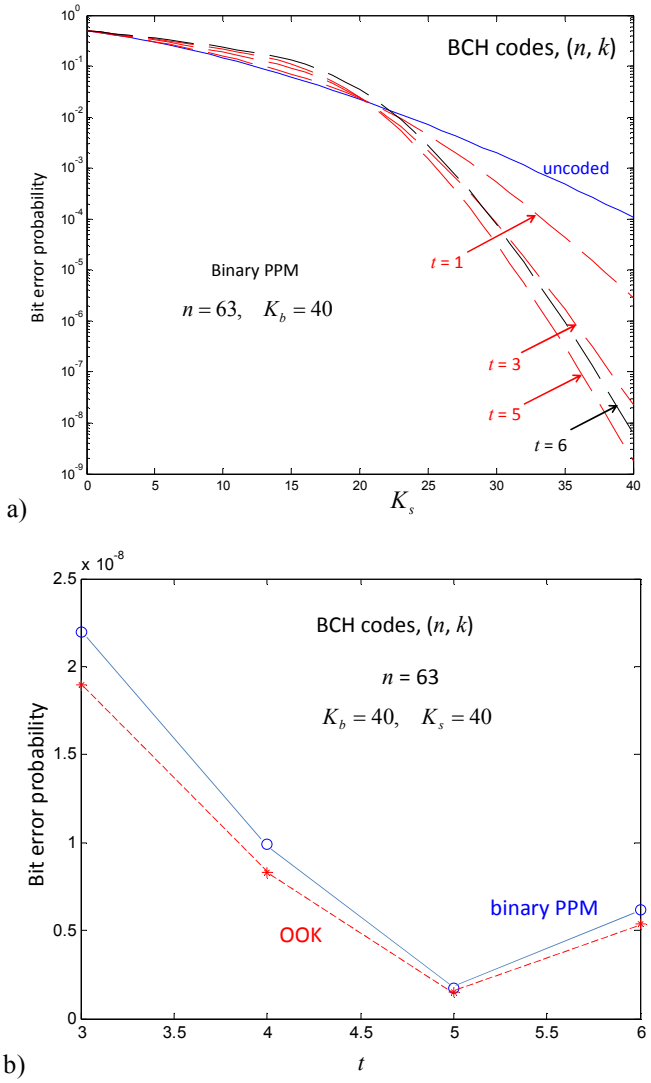

Fig. 9. a) Uncoded and BCH block-coded performance of binary PPM symbols for increasing error correction strength, with $n = 63$; b) minimum error probability achieved with $t = 5, n = 63$.

Similar behavior can be seen in Fig. 9a) for increasing t at fixed codeword length $n = 63$, but in this case the reversal actually starts near $K_s = 0$, instead of near the threshold. This is attributed to the fact that the scaling factor k / n decreases with increasing t, hence the signal energy per scaled codeword symbol decreases with increasing t, reducing the available signal energy which in turn leads to more uncorrected errors than would occur with slightly smaller t but greater signal energy. However, it should be noted that in both cases considered, the optimum point occurs at bit error probabilities that are lower than the usual

communications requirements of 10^{-6} can be met with careful selection of error correcting capability t and codeword length n, even with hard-decision BCH block codes. Soft-decision decoding further improves performance by a nominal 2 dB in terms of required signal energy, and even greater coding gains can be realized with powerful modern codes, at the cost of greater receiver complexity. However, these examples with BCH codes serve to demonstrate the performance improvements available through the use of coding, enabling the polished panel optical receiver to achieve low bit error probabilities at high data-rates, as required by future deep-space optical communications applications.

6. SUMMARY

The optical communications performance of large aperture polished-panel optical receivers has been evaluated using experimentally obtained point-spread functions, demonstrating that deep-space optical communications requirements can be achieved at high data-rates through proper selection of modulation formats and the application of coding, even in high background environments encountered when pointing the polished panel receiver close to the sun. It was shown that high-quality lightweight aluminum panels could be manufactured with surface accuracies sufficient to concentrate light into a small spot, that could be detected with large area photon-counting arrays enabling optical communications in the future. As part of this demonstration effort, an aluminum panel manufactured by Vertex Antennentechnic GmbH. was installed on the main reflector of the 34-meter antenna at DSS-13, and a large-sensor camera manufactured by Finger Lakes Instruments was installed into a weather-proof enclosure and mounted next to the subreflector, to record the point-spread function (PSF) generated by the polished panel. Data was collected while tracking the planets Jupiter, Venus, Mars and bright stars at night, and detailed images of the PSF with various antenna pointing offsets were obtained [2]. A mathematical model of the focal-plane energy distribution was developed and applied to the experimentally measured PSF in order to predict optical communications performance. It was shown that bandwidth-efficient OOK and binary PPM modulation formats can be employed to communicate from interplanetary distances even in high background environments when coding is applied, and optimum operating points were determined for minimizing the error probabilities. It was also shown that uncoded OOK modulation together with large area photon-counting detector arrays can be used to closely approach the quantum limit for binary signals in the absence of background, demonstrating that optical receivers employing light and low-cost polished aluminum panels are fundamentally equivalent to much more expansive diffraction-limited optical receivers in terms of optical communications performance, when properly designed modulations and detection strategies are employed.

Acknowledgments: The author would like to acknowledge the contributions of team member Philip Tsao for developing the computer interface, and for supporting the experiments to acquire the data used for characterizing the PSF of the polished panel at DSS-13.

The research described in this paper was carried out at the Jet Propulsion Laboratory, California Institute of Technology, under a contract with the National Aeronautics and Space Administration.

REFERENCES

[1] V. Vilnrotter, D. Hoppe, B. Moision, J. Charles, "Optical Communications Performance of Hybrid 34-meter Microwave Antennas," IEEE Aerospace Conference, Big Sky, MT, March 2010.

[2] V. Vilnrotter, "Experimental Evaluation of Optically Polished Panels on the Deep Space Network's 34 Meter Antenna," IEEE Aerospace Conference, Big Sky, MT, March 2012.

[3] V. Vilnrotter, M. Srinivasan, "Adaptive Detector Arrays for Optical Communications Receivers," IEEE Transactions on Communications, Vol. 50, Issue 7, 2002, pp. 1091-1097.

[4] Gagliardi and Karp, *Optical Communications*, John Wiley and Sons, New York, 1976.

[5] J. P. Odenwalder, "Error Control Coding Handbook," Linkabit Corp., San Diego, 15 July 1976.

[6] B. Sklar, "Digital Communications," Prentice Hall, New Jersey, 2001.

Biographies

Victor A. Vilnrotter *(M'79, SM'02) received his Ph.D. in electrical engineering and communications theory from the University of Southern California in 1978. He joined the Jet Propulsion Laboratory, Pasadena, Calif., in 1979, where he is a Principal Engineer in the Communication Architectures and Research Section. His research interests include electronic compensation of large antennas with focal-plane arrays, adaptive combining algorithms for large antenna arrays, optical communications through atmospheric turbulence, the application of quantum communications to deep-space optical links, and the development of uplink array calibration and tracking technologies. He has published extensively in conferences and refereed journals, and has received numerous NASA awards for technical innovations.*